OPEN ACCESS

ACTA METALLURGICA SLOVACA

2026, VOL. 32, NO. 1, 4-9

SCICELL

RESEARCH PAPER

Wear characteristics of artificial lumbar disc spine implant on various center of radius position

Lilik Dwi Setyana[1)], Suyitno[2)], Benidiktus Tulung Prayoga[1)], Handoko[1)], Wiyadi [1)], Arie Wibowo Kurniyawan[1)], Jad Farras Humaid[1)]*

[1)]*Department of Mechanical Engineering, Vocational College, Universitas Gadjah Mada, Yogyakarta, 55281, Indonesia*

[2)]*Department of Mechanical Engineering, Faculty of Engineering, Universitas Tidar, North Magelang, Indonesia*

*Corresponding author: lilikdwi_s@ugm.ac.id, tel.: +628562856934, Vocational College / Universitas Gadjah Mada, 55281, Yogyakarta, Indonesia

Received: 04.11.2025
Accepted: 12.01.2026

ABSTRACT

Various center of radius (CoR) positions has been applied in lumbar disc designs; however, their influence on wear performance remains unclear. This study investigates the effect of CoR position on the wear volume and surface roughness of an artificial lumbar disc implant. Wear tests were conducted using a UHMWPE ball against a CP-Ti artificial lumbar disc under dynamic loading up to 150 N for one million cycles. The tests involved flexion-extension, lateral bending, and axial rotation motions at different CoR positions (8, 10, and 12 mm). The wear volume of the CP-Ti component increased from 0.981 ± 0.076 to 2.011 ± 0.162 mm³/MC, while the surface roughness decreased from 0.512 ± 0.047 µm to 0.382 ± 0.039 µm as the CoR increased from 8 to 12 mm. Similarly, the wear rate of the UHMWPE ball increased from 7.86 ± 0.786 to 12.13 ± 0.605 mm³/MC, accompanied by a surface roughness reduction from 0.421 ± 0.0591 to 0.341 ± 0.0679 µm. The dominant wear mechanisms observed were ploughing, scratching, and abrasive wear. At a CoR of 10 mm, the wear volumes of CP-Ti and UHMWPE were 1.581 ± 0.206 and 9.97 ± 0.454 mm³/MC, respectively—values below 10 mm³/MC, meeting the standard for lumbar disc implant applications. Meanwhile, the surface roughness values of the CP-Ti and UHMWPE components were 0.382 ± 0.0481 µm, respectively. The artificial lumbar disc configuration with a CoR position of 10 mm demonstrated an optimal balance between contact pressure and contact area at the ball–plate interface. Therefore, a CoR 10 mm is recommended to achieve superior performance in lumbar disc implant applications.

Keywords: Center of radius, Wear volume, Commercial pure titanium, Lumbar disc, Implant

INTRODUCTION

Degenerative lumbar disc disease is a major cause of spinal disability and a source of neurological complications, significantly affecting human quality of life. For such diseases, artificial lumbar disc replacement has gained significant adoption over the past decade as an effective treatment for structural abnormalities and degenerative conditions of the lumbar intervertebral disc. Therefore, successful lumbar spine surgery must aim to restore physiological motion, maintain structural stability, and ensure long-term durability [1]. Total disc replacement (TDR) is an alternative to spinal fusion for the management of degenerative disc disease, aiming to preserve motion at the index level and reduce stress on adjacent segments [2-5]. Unlike fusion, which eliminates movement, TDR aims to maintain near-normal spinal kinematics, restore segmental function, provide lasting pain relief, and prevent adjacent segment degeneration [6].

Wear performance is a critical determinant of the longevity of articulating implants and is equally relevant to TDR devices. Inadequate wear resistance can compromise biomechanical function and elicit adverse biological responses to wear debris, potentially causing osteolysis and implant loosening [7–9]. Most TDRs adopt a ball-on-socket design, where friction between polyethylene and metal surfaces produces particulate debris and releases metal ions [10]. Both metal and polyethylene particles possess osteolytic potential [11,12], with debris in the 0.1–1.0 µm range being particularly active in triggering osteolytic cytokine activity [13].

In vitro wear simulations are an essential component of preclinical safety and performance assessments for spinal implants. These tests are typically performed under load and motion conditions that replicate physiological spinal movements [10], following standardized procedures such as ISO 18192-1 or ASTM F2423 [14,15]. Test parameters are selected to reflect spinal conditions, including motion patterns, lubrication, loading, and frequency [10]. Multidirectional loading is preferred for such simulations [16], and previous studies have shown that a frequency of 2 Hz generates greater wear compared to 1 Hz in lumbar disc testing [17]. However, further refinement of testing parameters is required to obtain reliable wear data [10]. Reported wear rates for TDR range from 1.12 to 20.76 mm³/MC [18], while optimal performance requires wear levels below 10 mm³/MC [19]. Efforts to reduce wear include modifying the center of radius (CoR) of the UHMWPE ball toward the socket endplate [20] and applying surface treatments [10,18,21].

Surface roughness and morphology play a pivotal role in the overall performance of orthopedic implants [22]. For instance, increasing the surface roughness of titanium-based implants has been shown to enhance osseointegration [23,24]. However, excessive roughness can adversely affect fatigue strength [25] and corrosion resistance [26,27], and increase the risk of bacterial adhesion on metallic biomaterials and biomedical implants [28]. Consequently, careful control of surface roughness and morphology during manufacturing is essential to ensure the longevity and functionality of metallic implants [22].

In wear simulations, the CoR of the lumbar disc is typically positioned at the center of the polyethylene core. Shifting the CoR below the disc center requires reevaluation to determine its impact on wear [20]. Previous studies have shown that relocating the CoR from the center of the UHMWPE core to the lower baseplate increases wear in unconstrained UHMWPE–CoCrMo ball-on-socket configurations [20]. Simulations with varying CoR positions are necessary to evaluate wear characteristics, particularly for particles smaller than 0.1 µm [29]. This study aims to identify the optimal CoR positions for an artificial lumbar disc to minimize wear under flexion–extension, lateral bending, and axial rotation. The findings are expected to serve as a design reference for ball-on-socket lumbar disc implants.

MATERIAL AND METHODS

Ball-on-Socket Model

The present study focuses on a lumbar disc implant (**Fig. 1**), which was simplified into a ball-and-socket configuration for experimental analysis (**Fig. 2**). The lumbar disc implant (**Fig. 1**) is composed of three components: the upper plate (a), the UHMWPE ball (b), and the lower plate (c). To model the frictional interaction between the upper plate and the UHMWPE ball, the system was reduced to two primary components. The upper component (ball) has a convex geometry and is fabricated from Ultra-High Molecular Weight Polyethylene (UHMWPE), while

the lower component (socket) has a concave geometry and is made of commercial pure titanium (CP-Ti), forming a spherical articulating interface. This simplification enables controlled evaluation of the contact mechanics and wear characteristics of the articulating pair. The ball-and-socket configuration represents load-bearing motion in the lumbar spine and is frequently used to assess tribological performance in artificial disc replacements.

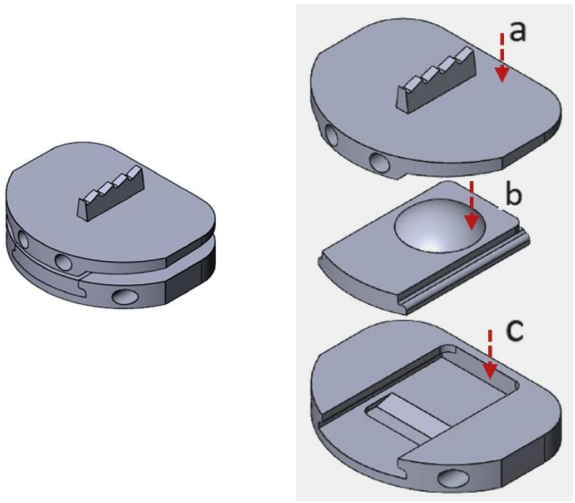

Fig. 1 The design of lumbar disc spine implant

Fig. 2(a) illustrates the schematic of the contact configuration between the UHMWPE ball and the CP-Ti artificial lumbar disc (ALD). **Fig. 2(b)** presents the variation in the distance between the lowest point of the socket's articulating surface and the CoR of the UHMWPE ball, designated as CoR 1, CoR 2, and CoR 3. The CoR positions for CoR 1, CoR 2, and CoR 3 are 8, 10, and 12 mm, respectively, measured from the central point of the endplate. The corresponding contact areas formed between the UHMWPE ball and the socket at CoR 1, CoR 2, and CoR 3 are 12.36 mm², 18.24 mm², and 36.10 mm², respectively. These contact areas were calculated based on the theoretical spherical surface contact area equation. As the CoR distance increases, the contact region expands, resulting in a broader load distribution across the articulating surfaces. This geometric variation is expected to influence both the contact pressure profile and the wear characteristics during articulation, thereby affecting the overall tribological performance of the implant.

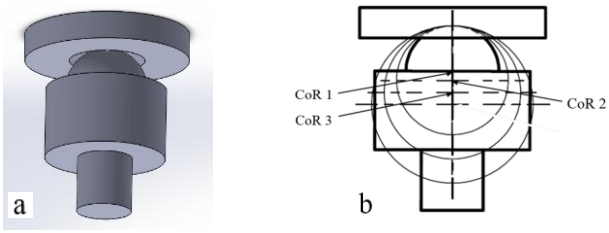

Fig. 2 The illustration schematic of the center of radius (CoR) ALD of the UHMWPE ball

The ball component was made of ultra-high molecular weight polyethylene, while the socket was fabricated from commercially pure titanium (CP-Ti). The CP-Ti primarily consisted of 99.75 wt.% titanium, 0.13 wt.% iron, and 0.12 wt.% gaseous elements. Composition analysis was performed using SEM-EDS (Quanta X50) and verified in accordance with ASTM A240/A240M standards. The CP-Ti ALD was produced via investment casting.

The specimens were sequentially polished using abrasive papers of grades #400, #800, and #2000, followed by polishing step with diamond paste to achieve an average surface roughness (Ra) of 0.10 ± 0.03 µm. Subsequently, all specimens were ultrasonically cleaned in distilled water for 20 minutes. This careful preparation ensured a smooth, contamination-free surface suitable for subsequent testing and analysis.

The insert ball was made of Ultra-High Molecular Weight Polyethylene, while the socket component was fabricated from commercial pure titanium. The primary composition of CP-Ti consists of 99.75 wt% Ti, 0.13 wt% Fe, and 0.12 wt% gas impurities. Elemental composition analysis was performed using SEM-EDS and the results were verified in accordance with the relevant ASTM specifications.

The CP-Ti ALD was produced using investment casting. The specimen surfaces were prepared by sequential grinding with #400, #800, and #2000 grit abrasive papers, followed by polishing with alumina paste to achieve an average surface roughness (Ra) of 0.10 ± 0.03 µm. All specimens were ultrasonically cleaned in distilled water for 20 minutes prior to testing. The surface preparation and cleaning procedures were conducted to minimize initial surface defects and ensure consistency in the tribological evaluation.

Wear Simulation Test

The wear resistance of the ALD was evaluated using a tribotester equipped with a three-station spinal simulator, specifically adapted to replicate spinal motions and loading conditions. The wear test simulation scheme is illustrated in **Fig. 3**. The motion parameters, including angle, frequency, and load—were determined in accordance with ISO 18192-1 (2011). The ALD was tested under axial-rotational (A/R) motion with an angular displacement of ±4°, as well as flexion-extension (F/E) and lateral-bending (L/B) motions with an angular displacement of ±7.5°. Motion control in the testing apparatus was operated via the Mach3 program. The wear test was conducted under lubrication with a mixture of 25 vol.% bovine serum and 75 vol.% aquades [1, 21, 22] to closely mimic in vivo conditions. The bovine serum contained 6.770 g/dL of protein and 2.757 g/dL of albumin. The wear resistance test was performed under a dynamic axial load of 50–150 N for up to 1 million cycles (MC) at 2 Hz.

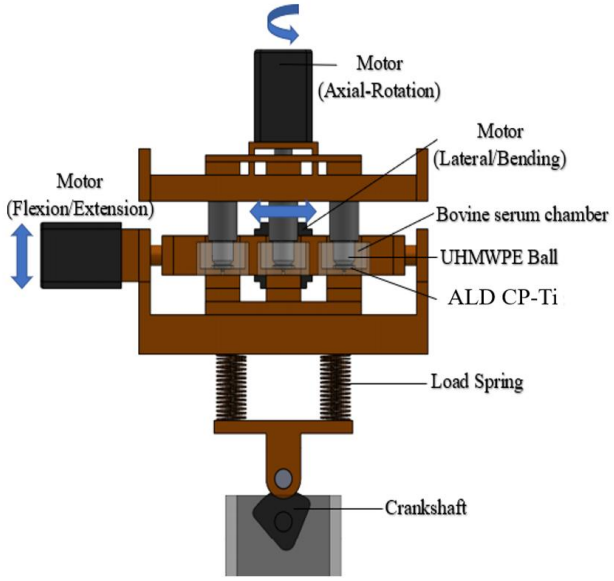

Fig. 3 The schematic of the wear tribotester

The UHMWPE balls were pre-soaked in bovine serum for two weeks, followed by storage at room temperature for 48 hours in order to limit fluid absorption and stabilize mass during the wear resistance test. The mass was measured using a digital balance with a resolution of 0.1 mg (Ohaus PA214C, USA). The ALD assembly was then placed inside a chamber installed on the tribotester. The test chamber was enclosed with an elastic membrane to avoid contamination of the bovine serum during the experiment. The specimens were periodically removed from the apparatus, ultrasonically cleaned, and weighed every 250.000 cycles (0.25 MC). Each specimen underwent wear testing up to a total of 1 MC. The surface morphology of the wear scars was observed using a stereozoom microscope (Olympus, Japan), and the post-test surface roughness (Ra) was measured with a profilometer (Fowler SE 1700).

RESULTS AND DISCUSSION

Results

Wear Volume

Fig. 4 presents the wear volume of the artificial lumbar disc made of CP-Ti with different center of rotation (CoR) positions. The wear volume increased linearly with the number of test cycles. Wear also increased with higher CoR positions. After 1 MC, the wear volumes at CoR positions of 8, 10, and 12 mm were 0.981 ± 0.076, 1.581 ± 0.206, and 2.011 ± 0.162 mm³/MC, respectively. The wear volume at CoR 8 mm was lower than that at CoR 12 mm. The percentage increase in wear volume up to 1 MC at CoR positions of 8, 10, and 12 mm was 48%, 64%, and 65%, respectively. The lowest wear rate from 0.25 MC to 1 MC was observed at the 12 mm CoR position.

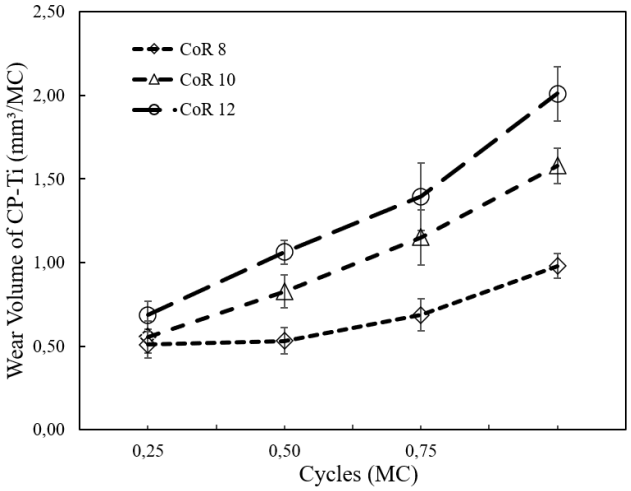

Fig. 4 The wear volume of the CP-Ti artificial lumbar disc

Fig. 5 presents the wear volume of UHMWPE at various CoR positions. Consistent with CP-Ti ALD, the UHMWPE wear volume increased linearly with the number of testing cycles. The farther the CoR position is from the center of the concavity, the higher the wear volume observed. After 1 MC, the wear volumes at CoR positions of 8, 10, and 12 mm were 7.86 ± 0.786, 9.97 ± 0.454, and 12.13 ± 0.605 mm³/MC, respectively. The differences in wear volume between 0.25 MC and 1 MC were nearly identical across all CoR variations, with increases of 32%, 40%, and 52% for CoR positions of 8, 10, and 12 mm, respectively. Moreover, the wear rate of UHMWPE was more than six times (6x) greater than that of the CP-Ti ALD. This result was lower than values reported in a previous study [10], primarily due to differences in the hardness of the two materials. The wear volume of the UHMWPE ball obtained in this study was comparable to the ISO standard (14.46 ± 2.1 mm³/MC), as reported by [29]. Wear occurred as the two surfaces were subjected to contact pressure and sliding motion. At the interface, asperity peaks generated scratches. After cyclic loading for a long period, the asperity peak fractured, and debris formed. The accumulation of debris further accelerated the wear process.

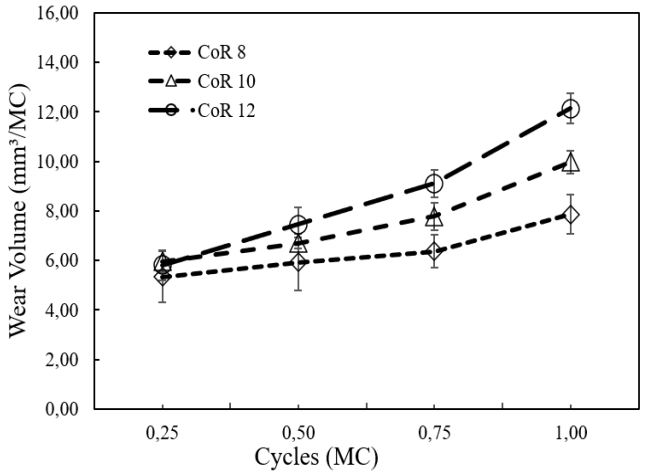

Fig. 5 The wear volume of the UHMWPE ball

Fig. 6 compares the wear volumes of UHMWPE ball and CP-Ti ALD. Both materials exhibited an increasing trend in wear rate with greater CoR distance from the center of the endplate ALD. The wear volumes of UHMWPE ball at CoR positions of 8, 10, and 12 mm were 8.01, 6.31, and 6.03 times higher, respectively, than those of CP-Ti ALD.

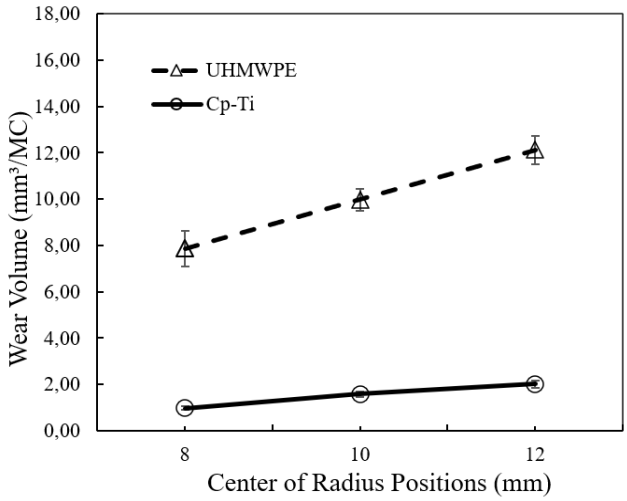

Fig. 6 The wear volume comparison of the UHMWPE ball and CP-Ti ALD

Surface Roughness

Fig. 7 presents the surface roughness of the articulating CP-Ti ALD surface after wear against the UHMWPE ball. Surface roughness is reported as the arithmetic mean roughness (Ra), measured at four randomly selected locations on each specimen. The results show that the surface roughness decreases as the CoR distance increases from 8 to 12 mm. For all CoR configurations, the surface roughness initially increases up to 0.50 million cycles (MC), decreases at 0.75 MC, and then increases progressively again up to 1 MC. The highest surface roughness was observed at 0.50 MC for the CoR 8 mm configuration (0.512 ± 0.047 µm), compared to 0.382 ± 0.039 µm for the CoR 12 mm configuration at the same cycle. After 1 million cycles, the surface roughness increased by 81% at a CoR of 8 mm and by 68% at a CoR of 12 mm. This indicates that specimens with smaller CoR values exhibited greater surface degradation under identical testing conditions.

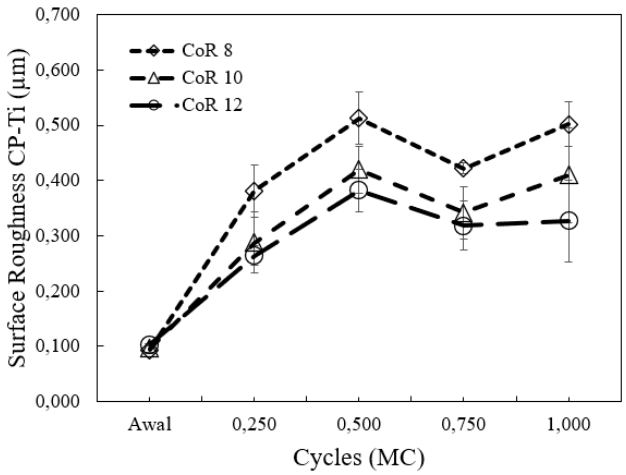

Fig. 7 The surface roughness of the CP-Ti artificial lumbar disc at different CoR positions during wear testing.

Fig. 8 shows the roughness of the UHMWPE ball in the regions that are articulated against the CP-Ti ALD for the different CoR positions. The surface roughness trends were consistent with those observed for the CP-Ti ALD. Specifically, surface roughness decreased as the CoR distance increased from 8 to 12 mm. For all CoR configurations, surface roughness initially increased with wear testing up to 0.50 million cycles (MC), then decreased at 0.75 MC, and then increased again as the wear test continued to 1 MC. The highest roughness values for CoR 8, 10, and 12 mm were observed at 0.50 MC. The percentage increase in surface roughness from the initial condition to 1 MC for CoR 8, 10, and 12 mm was 69%, 72%, and 75%, respectively. This behaviour suggests that early abrasive wear dominates up to 0.50 MC, likely due to initial asperity interactions. The subsequent decrease in roughness at 0.75 MC corresponds to a smoothing or burnishing effect as the contact surfaces conform. The later increase in roughness up to 1 MC is indicative of more aggressive wear once the contact stresses stabilize, particularly at smaller CoR distances where contact pressures are higher.

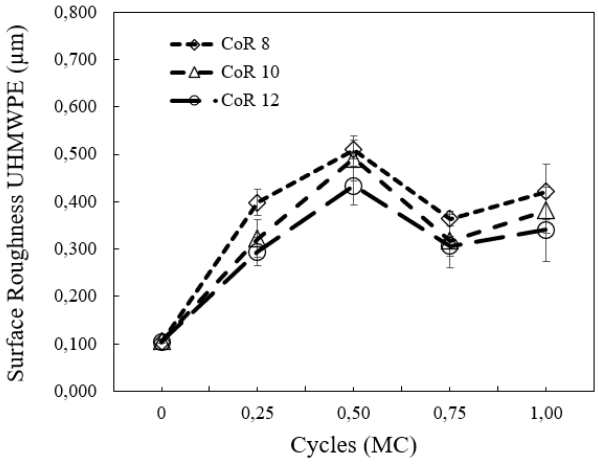

Fig. 8 The surface roughness of the UHMWPE ball at different CoR positions during wear testing

Wear Scars Observations

Wear scratch patterns in the central region of the CP-Ti ALD are presented in Fig. 9. The multi-directional wear testing, which included lateral-bending, axial-rotational, and flexion-extension motions, resulted in distinct variations in the wear track morphology. The wear tracks exhibit a combination of circular, linear, and arcuate patterns across the socket surface, indicating complex articulating kinematics. Overall, the wear paths appear irregular due to numerous intersecting scratches. At the CoR position of 8 mm, the wear scars are deeper and more irregular in direction (Fig. 9A). Small pit-like features are visible, indicating material removal in the form of debris detachment (hole debris). In contrast, at the CoR position of 12 mm, the wear scars are shallower and predominantly display radial patterns (Fig. 9B). The wear lines tend to radiate outward from the pole toward the perimeter of the socket. The more severe and disordered wear at smaller CoR distances suggests higher localized contact pressure and abrasive interaction, whereas larger CoR distances promote a more distributed load, resulting in smoother, radially aligned wear features.

Fig. 10 shows the wear scratches on the UHMWPE ball that articulated against the CP-Ti ALD. At the CoR position of 8 mm (**Fig. 10A**), the wear scars appear deep, with noticeable material removal, leading to debris detachment. In contrast, the wear scars at the CoR position of 12 mm (**Fig. 10B**) are shallower and show less material pull-out. The central region of the UHMWPE surface in direct contact with the CP-Ti ALD appears rougher than the surrounding areas. The surface roughness is attributed to scratch formation and localized gouging due to abrasive wear. The increase in surface roughness of the UHMWPE ball is associated with both abrasive wear and fatigue-induced surface damage, resulting from plastic deformation under cyclic, multi-directional loading. The deeper and more irregular wear at the smaller CoR indicates concentrated contact stress and more aggressive abrasion, whereas the shallower wear at larger CoR distances suggests a more evenly distributed load that reduces localized fatigue damage.

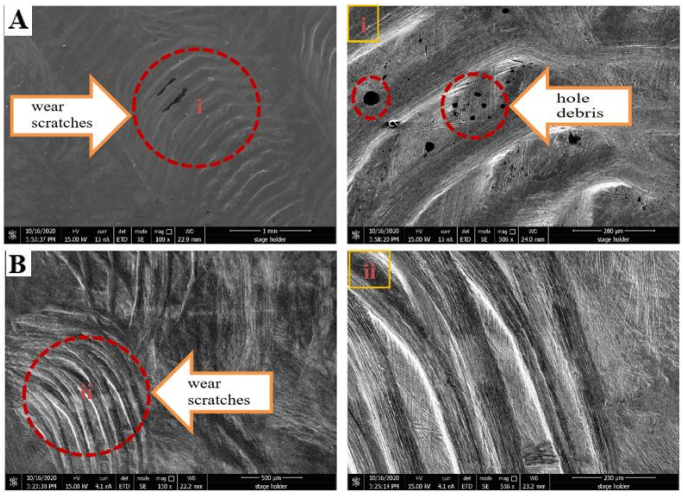

Fig. 9 The SEM micrographs of UHMWPE wear surfaces showing wear scratches and hole debris at different CoR positions

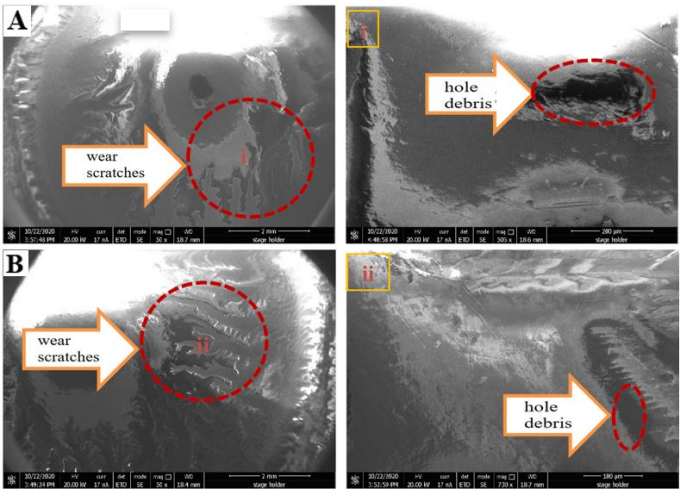

Fig. 10 The wear scar morphology on the central region of the UHMWPE ball at different CoR positions: (A) CoR = 8 mm and (B) CoR = 12 mm.

Microstructure

Fig. 11 shows the microstructure of the ALD product at both the surface and sub-surface regions. The microstructure is characterized by the presence of an α-phase matrix with remnants of prior β grains boundaries, which are consistent with previous studies [30, 31]. The identified features include the α-case (a), prior β grain boundaries (b), and α-Widmanstätten structure (c). The α-case layer is formed on the surface with a thickness of approximately 50–100 μm. Although the α-case exhibits high hardness, some regions contain crack tails with lengths of about 20–50 μm (d). Cracking in the α-case is characterized by intergranular fractures and smooth fracture surfaces, attributed to the presence of liquid phases in interdendritic regions during crack propagation. Crack formation takes place when the plastic strain at the solidus temperature exceeds the experimentally measured fracture strain within that temperature range. The susceptibility to cracking is further exacerbated by increased casting speeds. The likelihood of cracking increases with higher casting speeds. When the cavity diameter is below a critical value, microporosity develops; above this threshold, crack propagation occurs.

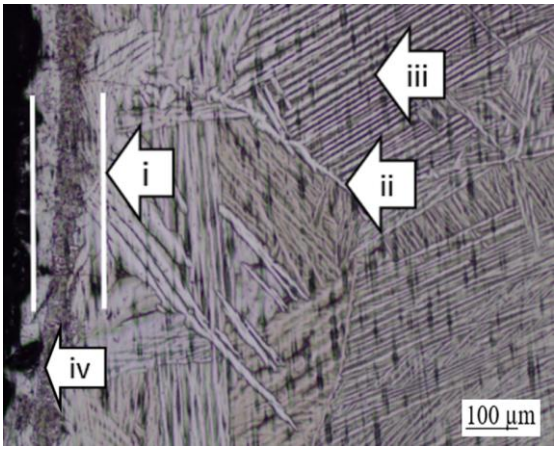

Fig. 11 The microstructure of the artificial lumbar disc CP-Ti [30]

Wear scratches resulting from contact with UHMWPE were observed on the surface. Some areas of the surface also exhibited material delamination, forming cavities that appeared as dark regions. In the subsurface region, the microstructure consisted of finer grains compared to the central region. These changes in microstructural size were influenced by the pressure and friction generated during the wear test. The β-prior grains exhibited an equiaxed morphology containing α plates. These plates were similar to the Widmanstätten-type α phase reported by [32]. Such grain morphology is also attributed to the slow cooling rate caused by the thickness of the mold wall [33]. A similar observation was reported by [34], who found that the as-cast microstructure of CP-Ti exhibited elongated, plate-like features due to slow cooling rates.

Discussion

The increase in CoR distance from the endplate center led to a higher wear volume in the ALD bearing pair. This trend is consistent with previous findings regarding the influence of CoR position on wear behavior [11]. As the CoR distance increased, the contact area between the ball and socket also increased. A larger contact area results in a wider frictional interface, thereby generating more wear debris. For example, the contact area at a CoR of 12 mm was 36.10 mm², which is approximately 2.92 times larger than the contact area at a CoR of 8 mm. Consequently, the contact stress at CoR 12 mm decreased by approximately the same factor (±2.92X) compared to the stress at CoR 8 mm. This behavior aligns with established wear models showing that wear coefficients decrease as contact stress is reduced [23]. The reduction in wear rate is therefore attributed to the larger surface area, which distributes the load over a larger frictional interface. Wear rate is also influenced by lubrication conditions [24], and an expanded contact interface promotes greater debris formation during articulation [25]. Conversely, a smaller CoR position produces a smaller contact area, leading to higher localized stresses and less debris formation due to the reduced surface interaction. These findings indicate that geometric configuration has a significant impact in regulating the balance between contact stress and contact area, which together determine the dominant wear mechanisms in UHMWPE CP-Ti articulating surfaces.

The difference in wear volume became more pronounced as the wear test progressed from 0.25 million cycles (MC) to 1 MC. These results indicate that increasing the number of sliding cycles progressively increases wear volume. In addition, prolonged articulation between the contact surfaces generates greater wear debris. The debris primarily originated from the UHMWPE ball, with a minor contribution from the CP-Ti ALD. The accumulated debris accelerated further wear, leading to the formation of third-body wear mechanisms.

The wear volume of UHMWPE balls after multidirectional motion testing (F/E, L/B, and A/R), which was approximately 6.4 times higher than the volumetric wear rate of the CP-Ti ALD. This result was lower than that reported in a previous study [12], primarily due to differences in the hardness of the two materials. The wear volume of the UHMWPE ball obtained in this study was nearly identical to the ISO standard (14.46 ± 2.1 mm³/MC), as reported in [20]. Wear occurred as the two surfaces were pressed and rubbed. At the interface, asperity peaks generate scratches, and under prolonged cyclic loading, they fracture, forming debris. The accumulation of debris further accelerated the wear process. This finding highlights the transition from mild to more severe wear conditions as the number of cycles increases, emphasizing the role of debris entrapment and circulation in promoting third-body abrasion.

The evolution of surface roughness for both the CP-Ti ALD and the UHMWPE ball during articulation can be categorized into three clearly defined stages: (i) surface roughening, (ii) surface smoothing, and (iii) saturation. This trend is consistent with previous studies [13]. In stage (i), surface roughness increases during the initial sliding period up to approximately 0.5 million cycles (MC), attributed to the formation of wear scratches on both the CP-Ti and UHMWPE surfaces. In stage (ii), surface roughness decreases as debris generation leads to third-body wear, which causes the asperity peaks to fracture and smooth out the surface. Finally, in stage (iii), saturation occurs when the surface roughness stabilizes and no longer changes significantly with continued wear testing.

The surface roughness of both the CP-Ti ALD and the UHMWPE ball decreased with increasing CoR distance from the endplate center. A smaller CoR position, located closer to the endplate center, resulted in a narrower contact area and consequently higher contact pressure. The increased pressure led to deeper wear scratches, which correlate with higher surface roughness values (**Fig. 10**). These findings are consistent with previous simulation results [25]. The surface roughness of the CP-Ti socket was primarily as consequence of ploughing and abrasive wear, while the roughness of the UHMWPE ball was attributed to adhesive and fatigue wear induced by plastic deformation under cyclic loading and multi-directional motions. The correlation between contact geometry and wear mechanism indicates that local stress concentration plays a dominant role in determining the prevailing wear mode and the resulting surface topography.

The ALD configuration with a CoR position of 8 mm exhibited a lower wear rate but higher surface roughness, whereas the CoR position of 12 mm showed a higher wear volume but lower surface roughness. For the CP-Ti ALD at a CoR of 10 mm, the wear volume and surface roughness were 1.581 ± 0.206 mm³/MC and 0.410 ± 0.0858 μm, respectively. The corresponding wear volume for the UHMWPE ball was 9.97 ± 0.454 mm³/MC, while the surface roughness was 0.382 ± 0.0481 μm. Furthermore, the CoR position located 10 mm from the center of the endplate demonstrated the most optimal distance between contact area and contact pressure at the ball–upper plate interface, indicating optimal load distribution and tribological performance. This balance reduced debris generation at the articulating surfaces under cyclic loading, thereby contributing to smoother surface topography and more stable tribological performance. These results suggest that the 10 mm CoR configuration achieves a favorable trade-off between wear volume and surface roughness, which could be beneficial for enhancing the long-term durability of lumbar disc implants.

CONCLUSION

The conclusions of this study are as follows:

1. The center of radius of the ball-on-socket pair significantly influences the wear behavior of the artificial lumbar disc. As the CoR increases, the wear rate tends to rise, while the surface roughness correspondingly decreases. This indicates that geometric alignment plays a crucial role in determining tribological performance and the distribution of contact stress. Therefore,

optimizing the CoR position is essential to achieve a balance between minimal wear and stable surface conditions.

2. The wear mechanisms of the CP-Ti ALD and UHMWPE ball were found to be similar across different CoR positions. The primary wear modes observed were scratching, plowing, and abrasive wear. These findings suggest that mechanical interaction between the metallic and polymeric components dominates the wear process, regardless of CoR variation. Further surface modification or lubrication strategies may be necessary to reduce these wear effects and enhance implant longevity.
3. Among the tested configurations, the CoR of 10 mm demonstrated the most favorable balance between wear volume and surface roughness, indicating that this geometry is suitable for application in lumbar disc implant designs.

Acknowledgments
This study was funded by the Directorate of Research and Community Service, Directorate General of Research and Development, Ministry of Higher Education, Science, and Technology. The authors would also like to express their sincere gratitude to Universitas Gadjah Mada for the research facilities that enabled the successful completion of this work.

REFERENCES

[1] J.K. Biswas, A. Malas, S. Majumdar, M. Rana: Computer Methods in Biomechanics and Biomedical Engineering, 25(16), 2022, 1812–1820. https:// doi.org/10.1080/10255842.2022.2039130
[2] P.A. Anderson, J.P. Rouleau: Spine, 29(23), 2004, 2779–2786. https:// doi.org/10.1097/01.brs.0000146460.11591.8a
[3] T.J. Errico: The Spine Journal, 4, 2004, 51S–157S. https://doi.org/10.1016/j.spinee.2004.07.004
[4] C.J. Neal, M.K. Rosner, T.R. Kuklo: Journal of Neurosurgery: Spine, 3(5), 2005, 342–347. https:// doi.org/10.3171/spi.2005.3.5.0342
[5] J.J. Regan, P.C. McAfee, R. Guyer, S.L. Blumenthal, F.H. Geisler: *Evaluation of the learning curve associated with artificial disc replacement: analysis from the prospective, randomized, multicenter FDA IDE study of the Charité artificial disc*, *Proceedings of the Spine Arthroplasty 5: Global Symposium on Motion Preservation Technology*, New York: Spine Arthroplasty Society, 2005.
[6] B.W. Cunningham, J.D. Gordon, A.E. Dmitriev, N. Hu, P.C. McAfee: *Spine*, 28(20), 2003, S110–S117. https://doi.org/10.1097/01.BRS.0000092209.27573.90
[7] D.A. Cavanaugh, P.D. Nunley, E.J. Kerr III, et al.: *Spine*, 34(7), 2009, E262–E265. https:// doi.org/10.1097/BRS.0b013e318195dd60
[8] B.W. Cunningham, C.M. Orbegoso, A.E. Dmitriev, et al.: The Spine Journal, 3(1), 2003, 19–32. https:// doi.org/10.1016/S1529-9430(02)00443-6
[9] R.D. Guyer, J. Shellock, B. MacLennan, D. Hanscom, R.Q. Knight, P. McCombe, et al.: Spine, 36(7), 2011, E492–E497. https://doi.org/10.1097/BRS.0b013e3181e9a4d2
[10] S. Wang, J. Song, Z. Liao, P. Feng, W. Liu: Materials Science and Engineering: C, 63, 2016, 256–265. https://doi.org/10.1016/j.msec.2016.02.070
[11] V.B. Susan, G. Jill, X.C. Wei, et al.: Journal of Orthopaedic Research, 22, 2004, 6–12. https:// doi.org/10.1016/S0736-0266(03)00153-0
[12] R.M. Hall, et al.: Journal of Engineering Tribology, 220(J8), 2006, 775–786. https:// doi.org/10.1243/13506501JET187
[13] E. Ingham, J. Fisher: Proceedings of the Institution of Mechanical Engineers, Part H: Journal of Engineering in Medicine, 214(1), 2000, 21–37. https:// doi.org/10.1243/0954411001535219
[14] ISO 18192-1: *Implants for surgery – Wear of total intervertebral spinal disc prostheses – Part 1: Loading and displacement parameters for wear testing and corresponding environmental conditions for tests*, The International Organization for Standardization, Geneva, Switzerland, 2011.
[15] ASTM F2423-11: *Standard guide for functional, kinematic, and wear assessment of total disc prostheses*, *Annual Book of ASTM Standards*, Vol. 13.01, ASTM International, 2011, p. 1–9.
[16] T.M. Grupp, H.J. Meisel, J.A. Cotton, et al.: Biomaterials, 31, 2010, 523–531. https:// doi.org/10.1016/j.biomaterials.2009.09.064
[17] A. Kettler, M. Bushelow, H.J. Wilke: European Spine Journal, 21, 2012, S709–S716. https://doi.org/10.1007/s00586-010-1582-8.
[18] R. Vicars, P. Prokopovich, T.D. Brown, J.L. Tipper, E. Ingham, J. Fisher, R.M. Hall: Spine, 37(9), 2012, E528–E534. https://doi.org/10.1097/BRS.0b013e31823cbd6e
[19] J. Fisher: Faraday Discussions, 156, 2012, 59–68. https://doi.org/10.1039/C2FD00001F
[20] P.J. Hyde, J. Fisher, R.M. Hall: Journal of Biomedical Materials Research Part B: Applied Biomaterials, 105(1), 2015, 46–52. https://doi.org/10.1002/jbm.b.33456
[21] J. Song, Y. Liu, Z. Liao, S. Wang, R. Tyagi, W. Liu: Materials Science and Engineering: C, 69, 2016, 985–994. https://doi.org/10.1016/j.msec.2016.08.007
[22] B. Arifvianto, M. Mahardika, U.A. Salim, Suyitno: Journal of Engineering and Technological Sciences, 52(1), 2020, 1–13. https://doi.org/10.5614/j.eng.technol.sci.2020.52.1.1
[23] N.E. Elias, Y. Oshida, J.H.C. Lima, C.A. Muller: Journal of the Mechanical Behavior of Biomedical Materials, 1, 2008, 234–242. https://doi.org/10.1016/j.jmbbm.2007.12.002
[24] L.L. Guehennec, A. Soueidan, P. Layrolle, Y. Amouriq: Dental Materials, 23(7), 2007, 844–854. https://doi.org/10.1016/j.dental.2006.06.025
[25] M. Baleani, M. Viceconti, A. Toni: Artificial Organs, 24(4), 2000, 296–299. https:// doi.org/10.1046/j.1525-1594.2000.06486.x
[26] G.L. Song, Z.Q. Xu: Electrochimica Acta, 55(13), 2010, 4148–4161. https:// doi.org/10.1016/j.electacta.2010.02.068
[27] Suyitno, B. Arifvianto, T.D. Widodo, M. Mahardika, P. Dewo, U.A. Salim: International Journal of Minerals, Metallurgy, and Materials, 19(12), 2012, 1093–1099. https:// doi.org/10.1007/s12613-012-0676-1
[28] Y.H. An, R.J. Friedmann: Journal of Biomedical Materials Research, 43(3), 1998, 338–348. https:// doi.org/10.22203/eCM.v008a05
[29] P.J. Hyde, J. Tipper, J. Fisher, R.M. Hall: Journal of the Mechanical Behavior of Biomedical Materials, 44, 2014, 43–52. https://doi.org/10.1016/j.jmbbm.2014.12.001
[30] L.D. Setyana, M. Mahardika, Suyitno: Acta Metallurgica Slovaca, 26(3), 2020, 132-137. https://doi.org/10.36547/ams.26.3.535
[31] K.M. Ibrahim, M. Mhaede, L. Wagner: Transactions of Nonferrous Metals Society of China, 21(8), 2011, 1735–1740. https://doi.org/10.1016/S1003-6326(11)60912-3
[32] M.J. Bermingham, S.D. McDonald, M.S. Dargusch, D.H. StJohn: Journal of Materials Research, 23(1), 2008, 97–104. https://doi.org/10.1557/JMR.2008.0013
[33] S.W. Xu, K.O. Ishi, S. Kamado, H. Takahashi, T. Homma: Materials Science and Engineering: A, 542, 2012, 71–78. https://doi.org/10.1016/j.msea.2012.02.091
[34] H. Attar, K.G. Prashanth, A.K. Chaubey, M. Calin, L.C. Zhang, S. Scudino, J. Eckert: Materials Letters, 142, 2015, 38–41. https://doi.org/10.1016/j.matlet.2014.11.153